Condensation of Steam Bubbles Injected into Sub-Cooled Water

D. Lucas and M. Beyer
Forschungszentrum Dresden-Rossendorf e.V., Institut of Safety Research
P.O.Box 510 119, 01314 Dresden, Germany
D.Lucas@fzd.de, M.Beyer@fzd.de

T. Frank
ANSYS Germany GmbH
Staudenfeldweg 12, D-83624 Otterfing, Germany
Thomas.Frank@ansys.com

P. Zwart
ANSYS Canada Ltd.
554 Parkside Drive, Waterloo, Ontario N2L 5Z4, Canada
Phil.Zwart@ansys.com

A. Burns
ANSYS UK Ltd.
West Central 127, Milton Park, Abingdon, OX14 4SA, UK
Alan.Burns@ansys.com

ABSTRACT

Bubble condensation plays an important role e.g. in sub-cooled boiling or steam injection into pools. Since the condensation rate is proportional to the interfacial area density, bubble size distributions have to be considered in an adequate modeling of the condensation process. The effect of bubble sizes was clearly shown in experimental investigations done previously at the TOPFLOW facility of FZD. Steam bubbles were injected into a sub-cooled upward pipe flow via orifices in the pipe wall located at different distances from measuring plane. 1 mm and 4 mm injection orifices were used to vary the initial bubble size distribution. Measurements were done using a wire-mesh sensor. Condensation is clearly faster in case of the injection via the smaller orifices, i.e. in case of smaller bubble sizes. In a previous work a simplified test solver, developed especially to test models for vertical pipe flow was used to simulate these effects. Now the results will be transferred to the CFD code CFX from ANSYS. Recently the Inhomogeneous MUSIG model was implemented into the code enabling the simulation of poly-dispersed flows including the effects of separation of small and large bubbles due to bubble size dependent lift force inversion. It allows to divide the dispersed phase into size classes regarding the mass as well as regarding the momentum balance. Up to now transfers between the classes in the mass balance can be considered only by bubble coalescence and breakup (population balance). Now an extension of the model is proposed to include the effects due to phase transfer. The paper focuses on the derivation of equations for the extension of the Inhomogeneous MUSIG model and presents a new experimental setup for the investigation on steam bubble condensation.

KEYWORDS

two-phase flow, condensation, bubble, CFD

1. INTRODUCTION

Computational Fluid Dynamics (CFD) simulations are increasingly used for analyses on special questions in Nuclear Reactor Safety (NRS). While a satisfying status is achieved for 3-dimensional simulations for single phase flows, e.g. for problems connected with boron mixing [1], still much effort is required to qualify CFD-codes for two-phase flows. Applying the two- or multi-fluid model (Euler-Euler) - which is the first choice for bubbly flows with high gas volume fraction and large simulation domains – all information on mass, momentum and energy transfer between the phases has to be implemented by so-called closure models. Due to the complexity of the interface and the large number of phenomena which have to be considered and which are highly interrelated, these models are not mature. Experimental data with high resolution in space and time are required to develop, improve and validate such models.

Typical examples for the relevance of bubble condensation in NRS are sub-cooled boiling in core cooling channels or emergency cooling systems, steam injection into pools or steam bubble entrainment into sub-cooled liquids by impinging jets, e.g. in case of Emergency Core Cooling Injection (ECC) into a partially uncovered cold leg [2]. All these cases are connected with pronounced 3-dimensional flow characteristics, i.e. adequate simulations require the application of CFD codes.

Many activities were done in the last years to improve the modeling of adiabatic bubbly flows in the frame of CFD. In this case models for momentum transfer between the phases are most important. Usually they are expressed as so-called bubble forces. Experimental investigation as well as Direct Numerical Simulations (DNS) showed, that these bubble forces strongly depend on the bubble size. In addition to the well known drag force also virtual mass, lift, turbulent dispersion and wall forces have to be considered [3]. The lift forces even changes its sign in dependence of the bubble size [4]. In consequence large bubbles are pushed to the opposite direction than small bubbles if a gradient of the liquid velocity perpendicular to the relative bubble velocity exists [5, 6]. To simulate the separation of small and large bubbles more than one momentum equation is required [7]. For this reason recently so-called Inhomogeneous-MUSIG (MUlti SIze Group) model was implemented into the ANSYS-CFX code [8, 9]. It allows the consideration of a number of bubble classes independently for the mass balance (for a proper modeling of bubble coalescence and breakup a large number of bubble groups is required) and for the momentum balance (only very few classes can be considered due to the high computational effort, criteria for the classification can be derived from the dependency of the bubble forces on the bubble size, e.g. the change of the sign of the lift force). In the presently implemented version of the Inhomogeneous MUSIG model only transfers between the bubble classes due to bubble coalescence and breakup can be modeled. In case of flows with phase transfer additional transfers between the single classes and the liquid and transfers between bubble classes caused by growth or shrinking of bubbles have to be considered. The equations for the extension of the MUSIG models are derived in Section 2.2 of this paper. They were recently implemented into the CFX code and are presently verified.

These extensions of the Inhomogeneous MUSIG model will allow to simulate flows with phase transfer in principle. However, for a simulation based on physics in addition proper closure models for evaporation and condensation rates are required. Usually these phase transfer rates are assumed to be proportional to the interfacial area density and the overheating or sub-cooling, respectively. For this reason detailed information on the evolution of local

bubbles size distributions and local temperature profiles is needed. In the past wire-mesh sensors were successfully used to measure local bubble size distributions in air-water [10] and adiabatic steam-water [6] flows in a vertical pipe. These data were used to validate models for bubble forces and to some extent also models bubble coalescence and breakup. While the available models for bubble forces provide an acceptable agreement with the experimental observations for a wide range of flow conditions the applicability of models for bubble coalescence and breakup is still limited [9]. First experiments using the wire-mesh sensor technology to investigate bubble condensation in an upwards vertical pipe were also done. They clearly showed the effect of interfacial area density by comparison of experimental results for which only the initial bubble size distribution was modified by using different orifice sizes for bubble injection, but keeping the gas and liquid flow rates constant [11]. Nevertheless these experiments had some preliminary character and some shortcomings due to the limited temperature measurement, the availability of only one wire-mesh sensor (not allowing to determine the gas velocity – see Chapter 3) and also due to the set pressure boundary condition. Learning from these test now new experiments are conducted. The new experimental setup and preliminary results are presented in Chapter 3 and 4, respectively. The paper has two main objectives: the derivation of the equations for the extension of the Inhomogeneous MUSIG model and the presentation of the new experimental setup which will provide experimental data suitable for the validation of the extended model.

2. EXTENSION OF THE INHOMOGENEOUS MUSIG MODEL

2.1 The Inhomgeneous MUSIG model

The inhomogeneous multiple size group (MUSIG) model which bases on multi-fluid Euler–Euler approach has been implemented recently into the CFX code from ANSYS [8, 9]. In this model the gaseous disperse phase is divided into a number N so-called velocity groups (or phases), where each of the velocity groups is characterized by its own velocity field. The subdivision should be based on the physics of bubble motion for bubbles of different size, e.g. different behavior of differently sized bubbles with respect to lift force (according to Tomiyama [4] the lift force changes its sign with increasing bubble size) or turbulent dispersion. Therefore in most cases two to four velocity groups should be sufficient in order to capture the main phenomena in bubbly or slug flows. Further the overall bubble size distribution is represented by dividing the bubble diameter range within each of the velocity groups in a number M_j bubble size classes. The lower and upper boundaries of bubble diameter intervals for the bubble size classes can be controlled by either an equal bubble diameter distribution, an equal bubble mass distribution or can be based on user definition of the bubble diameter ranges for each distinct bubble diameter class. Internally the conservation equations are formulated related on a discretisation regarding mass, i.e. bubble size group boundaries are characterized by a fixed bubble mass.

The Eulerian modeling framework is based on ensemble-averaged mass and momentum transport equations for all phases/velocity groups. Regarding the liquid phase as continuum (j = 1) and the gaseous phase velocity groups (bubbles) as disperse phase (j = 2, . . ., N+ 1) these equations for adiabatic conditions read:

$$\frac{\partial}{\partial t}\left(\alpha_j \rho_j\right)+\nabla\cdot\left(\alpha_j \rho_j \vec{U}_j\right)=S_j \tag{1}$$

$$\frac{\partial}{\partial t}\left(\alpha_j \rho_j \vec{U}_j\right)+\nabla\cdot\left(\alpha_j \rho_j \vec{U}_j\otimes\vec{U}_j\right)=\nabla\cdot\left(\alpha_j \mu_j\left(\nabla\vec{U}_j+\left(\nabla\vec{U}_j\right)^T\right)\right)-\alpha_j\nabla p+\alpha_j\rho_j\vec{g}+\vec{F}_j+\vec{S}_{Mj} \tag{2}$$

with $\vec{F}_j = \vec{F}_{j,D} + \vec{F}_{j,L} + \vec{F}_{j,W} + \vec{F}_{j,TD} + \vec{F}_{j,VM}$ (3)

where α_j, ρ_j, μ_j, U_j are the void fraction, density, viscosity and velocity of the phase j and F_j represents the sum of interfacial forces ($F_{j,D}$ drag force, $F_{j,L}$ lift force, $F_{j,W}$ wall lubrication force, $F_{j,TD}$ turbulent dispersion force and $F_{j,VM}$ virtual mass force).

The source terms S_j and S_{Mj} represent the transfer of gaseous phase mass and momentum between different velocity groups due to bubble break-up and coalescence processes leading to bubbles of certain size belonging to a different velocity group. Consequently these terms are zero for the liquid phase transport equations.

In the inhomogeneous MUSIG model each phase representing a velocity group of the gaseous phase is again subdivided in M_j size groups (= MUSIG groups), each representing a range of bubble sizes and where break-up and coalescence between all size groups is taken into account. Introducing ρ_G gas density and $\alpha_i = f_i * \alpha_j$ as the gas volume fraction of the MUSIG group i (with i = 1 … $\sum_{j=1}^{N} M_j$), which belongs to the velocity group j continuity equation for this group reads:

$$\frac{\partial}{\partial t}(\rho_g(\vec{r},t)\alpha_i(\vec{r},t)) + \frac{\partial}{\partial \vec{r}}(U_j(\vec{r},t)\rho_g(\vec{r},t)\alpha_i(\vec{r},t)) = m_i\left[B_{B,i}(\vec{r},t) - D_{B,i}(\vec{r},t) + B_{c,i}(\vec{r},t) - D_{c,i}(\vec{r},t)\right]. \quad (4)$$

where $B_{B,i}$ and $B_{C,i}$ are the bubble birth rates due to breakup of larger bubbles into size group i and coalescence of smaller bubbles to MUSIG group i, respectively. $D_{B,i}$ and $D_{C,i}$ are the bubble death rates due to breakup of bubbles from MUSIG group i into smaller bubbles and the coalescence of bubbles from size group i with other bubbles to even larger ones.

2.2 Extension of the Inhomogeneous MUSIG model to consider phase transfer

As shown in the previous section up to now only transfers between the bubble size groups due to bubble coalescence and breakup are considered. To simulate poly-dispersed flows with phase transfer additional source and sink terms due to evaporation or condensation have to added to eq. (4). There are in general three phenomena which have to be considered:

a) shrinking or expansion of bubbles due to temporal and spatial changes pressure,
b) direct mass transfer between the liquid phase and bubble size group i and
c) shrinking or expansion of bubbles due to mass transfer.

Since the bubble size group discretisation is done based on fixed mass bins no additional source terms arise from pressure changes. The product $\rho_g * \alpha_j$ remains constant. This means the presently implemented Inhomogeneous MUSIG model can be applied in principle also for cases which include changes of pressure. But it is important to mention that in such cases a discretisation of bubble size groups based on bubble diameter is variable in space and time, i.e. at different locations and different problem times the group boundaries in terms of bubble diameter may be different.

In case of phase transfer an additional source term $\Gamma_i(\vec{r},t)$ [kg/(m^{3}s)] has to be added to the right hand side of eq. (4) considering the direct mass transfer per unit volume and time between the continuous liquid phase and bubble size group i, at location $\vec{r}$ and time t. Γ_i can be calculated from the volume related heat flux to the interface and heat of evaporation [11]:

$$\Gamma_i = \frac{a_i}{H_{\mathrm{lg}}}\left(h_{g,i}(T_g - T_s) + h_{l,i}(T_l - T_s)\right) \tag{5}$$

Herein T_g, T_l and T_s are the gas, liquid and saturation temperatures, a_i is the interfacial area density of bubble size class i, H_{lg} the heat of evaporation and $h_{g,i}$ and $h_{l,i}$ are the heat transfer coefficients from the gas and liquid side to the interface formed from bubbles of the size group i.

Let's now consider the bubble number density $n(m, \vec{r}, t)$ [1/(m^3kg)] related to the bubble mass m. The corresponding balance equation reads:

$$\frac{dn(m,\vec{r},t)}{dt} = \frac{\partial}{\partial t} n(m,\vec{r},t) + \frac{\partial}{\partial \vec{r}}(U(m,\vec{r},t)n(m,\vec{r},t)) + \frac{\partial n(m,\vec{r},t)}{\partial m}\frac{\partial m(\vec{r},t)}{\partial t} = \tilde{B}_B(m,\vec{r},t) - \tilde{D}_B(m,\vec{r},t) + \tilde{B}_c(m,\vec{r},t) - \tilde{D}_c(m,\vec{r},t) \tag{6}$$

Herein $\tilde{B}$ and $\tilde{D}$ are the birth and death rates analogues to eq. (4), but related to the bubble mass. Since n depends on mass the total differential leads to an additional term. Physically it describes the shift of the particles along the mass coordinate, i.e. the particle shrinking or growth connected with the mass transfer.

Now a discretisation regarding MUSIG groups is introduced, i.e. eq. (5) has to be integrated over the mass of MUSIG group i. This yields an equation for the bubble number density of bubble size group i:

$$N_i(\vec{r},t) = \int_{m_{i-1/2}}^{m_{i+1/2}} n(m,\vec{r},t)\,dm \tag{7}$$

where $m_{i-1/2}$ and $m_{i+1/2}$ are the lower and upper boundaries of the size group I, respectively.

Assuming, that the MUSIG group i belongs to velocity group j the integration of eq. (6) results in:

$$\frac{dN_i(\vec{r},t)}{dt} = \frac{\partial}{\partial t} N_i(\vec{r},t) + \frac{\partial}{\partial \vec{r}}(U_j(\vec{r},t)N_i(\vec{r},t)) + \int_{m_{i-1/2}}^{m_{i+1/2}} \frac{\partial n(m,\vec{r},t)}{\partial m}\frac{\partial m(m,\vec{r},t)}{\partial t}\,dm = \int_{m_{i-1/2}}^{m_{i+1/2}} \left[\tilde{B}_B(m,\vec{r},t) - \tilde{D}_B(m,\vec{r},t) + \tilde{B}_c(m,\vec{r},t) - \tilde{D}_c(m,\vec{r},t)\right] dm \tag{8}$$

While the integration of the right-hand side provides the birth and death rates due to bubble coalescence and breakup for each size group i as introduced in eq. (4), the integral on the left-hand side can be expressed analogous to [12] as:

$$\int_{m_{i-1/2}}^{m_{i+1/2}} \frac{\partial n(m,\vec{r},t)}{\partial m}\frac{\partial m(m,\vec{r},t)}{\partial t}\,dm = \left[\frac{\partial m(m,\vec{r},t)}{\partial t} n(m,\vec{r},t)\right]_{m_{i-1/2}}^{m_{i+1/2}} - \int_{m_{i-1/2}}^{m_{i+1/2}} n(m,\vec{r},t)\frac{\partial}{\partial m}\frac{\partial m(m,\vec{r},t)}{\partial t}\,dm = \left[\frac{\partial m(m,\vec{r},t)}{\partial t} n(m,\vec{r},t)\right]_{m_{i-1/2}}^{m_{i+1/2}} - \int_{m_{i-1/2}}^{m_{i+1/2}} n(m,\vec{r},t)\frac{\partial}{\partial t}\frac{\partial m(m,\vec{r},t)}{\partial m}\,dm = \left[\frac{\partial m(m,\vec{r},t)}{\partial t} n(m,\vec{r},t)\right]_{m_{i-1/2}}^{m_{i+1/2}} \tag{9}$$

This term reflects the fact, that bubbles arrive in group i or leave the mass group i due to their growth or shrinking. Assuming a constant mass transfer rate within mass group i, it has to be distinguished between two cases:

$\left.\frac{\partial m(m,\vec{r},t)}{\partial t}\right|_i > 0$ (evaporation):

$$\tilde{S}_{i-1/2} = -\left.\frac{\partial m(m,\vec{r},t)}{\partial t}\right|_{i-1} \frac{N_{i-1}(\vec{r},t)}{m_i - m_{i-1}}, \quad \tilde{S}_{i+1/2} = \left.\frac{\partial m(m,\vec{r},t)}{\partial t}\right|_i \frac{N_i(\vec{r},t)}{m_{i+1} - m_i} \tag{10}$$

$\left.\frac{\partial m(m,\vec{r},t)}{\partial t}\right|_i < 0$ (condensation):

$$\tilde{S}_{i-1/2} = -\left.\frac{\partial m(m,\vec{r},t)}{\partial t}\right|_{i} \frac{N_i(\vec{r},t)}{m_i - m_{i-1}}, \quad \tilde{S}_{i+1/2} = \left.\frac{\partial m(m,\vec{r},t)}{\partial t}\right|_{i+1} \frac{N_{i+1}(\vec{r},t)}{m_{i+1} - m_i} \tag{11}$$

Now these source terms are shifted to the right-hand side of eq. (8). Multiplying with the mass of size group i m_i and considering $m_i * N_i = \rho_g * \alpha_i$ yields:

$$\frac{d(\rho_g(\vec{r},t)\alpha_i(\vec{r},t))}{dt} = \frac{\partial}{\partial t}(\rho_g(\vec{r},t)\alpha_i(\vec{r},t)) + \frac{\partial}{\partial \vec{r}}(U_j(\vec{r},t)\rho_g(\vec{r},t)\alpha_i(\vec{r},t)) = \\ m_i\left[B_{B,i}(\vec{r},t) - D_{B,i}(\vec{r},t) + B_{c,i}(\vec{r},t) - D_{c,i}(\vec{r},t)\right] + S_i(\vec{r},t) \tag{12}$$

with

$$S_i = -m_i(\tilde{S}_{i-1/2} + \tilde{S}_{i+1/2}) = m_i \left.\frac{\partial m(m,\vec{r},t)}{\partial t}\right|_{i-1} \frac{N_{i-1}(\vec{r},t)}{m_i - m_{i-1}} - m_i \left.\frac{\partial m(m,\vec{r},t)}{\partial t}\right|_i \frac{N_i(\vec{r},t)}{m_{i+1} - m_i} = \\ \rho_g\left[\frac{m_i}{m_{i-1}(m_i - m_{i-1})} \left.\frac{\partial m(m,\vec{r},t)}{\partial t}\right|_{i-1} \alpha_{i-1}(\vec{r},t) - \frac{1}{m_{i+1} - m_i} \left.\frac{\partial m(m,\vec{r},t)}{\partial t}\right|_i \alpha_i(\vec{r},t)\right] \tag{13}$$

for evaporation. To relate this source term to the previously introduced source term Γ_i the following relation is used:

$$\Gamma_i = \left.\frac{\partial m(m,\vec{r},t)}{\partial t}\right|_i \frac{1}{V} = \left.\frac{\partial m(m,\vec{r},t)}{\partial t}\right|_i \frac{\alpha_i}{V_{g,i}} = \left.\frac{\partial m(m,\vec{r},t)}{\partial t}\right|_i \frac{\alpha_i \rho_g}{m_i}. \tag{14}$$

with the volume of bubbles of group i $V_{g,i}$. The combination of eqs. (13) and (14) yields:

$$S_i = \frac{m_i}{m_i - m_{i-1}}\Gamma_{i-1} - \frac{m_i}{m_{i+1} - m_i}\Gamma_i \qquad \text{for} \quad \Gamma_i > 0 \quad \text{(evaporation).} \tag{15}$$

Analogue for condensation is obtained:

$$S_i = \frac{m_i}{m_i - m_{i-1}}\Gamma_i - \frac{m_i}{m_{i+1} - m_i}\Gamma_{i+1} \qquad \text{for} \quad \Gamma_i < 0 \quad \text{(condensation).} \tag{16}$$

These source terms reflect the effect of direct mass transfer between liquid and bubble size group i as well as the transfer between MUSIG groups due to bubble growth or shrinking. This can be checked by considering the net transfer at the group boundary. In case of condensation bubble sizes shrink, i.e. bubbles are shifted to smaller mass groups. Considering the net transfer at the lower boundary of bubble size group i $S_{i-1/2}$ there is a sink in bubble size group i according the eq. (16) $S_i = \frac{m_i}{m_i - m_{i-1}}\Gamma_i$ (Γ_i is negative in case of condensation). On the other hand the related source in bubble size group i-1 is $S_{i-1} = -\frac{m_{i-1}}{m_i - m_{i-1}}\Gamma_i$. Summation of gain and loss results in $S_{i-1/2} = \frac{m_i - m_{i-1}}{m_i - m_{i-1}}\Gamma_i = \Gamma_i$.

The set of eqs. (5), (12), (15) and (16) allows the simulation of poly-dispersed bubbly flows with phase transfer using a correlation for the heat transfer coefficients in eq. (5). It should be considered, that bubbles larger ~1 mm volume equivalent diameter are considerably deformed what clearly increases the interfacial area concentration compared to the one obtained for spherical bubbles. If the bubbles are not too large, empirical correlations as e.g. the one from Wellek et al. (1966) can be used.

On the other hand such an approach considerably increases the number of variables that have to be stored, since Γ_i is a field depending on space and bubble size. For this reason in a first implementation of the model extensions spherical bubbles are assumed. The Sauter mean diameter for the velocity group j is obtained according to:

$$D_{s,j} = \frac{\alpha_j}{\sum_{i}^{(i\subset j)} \frac{\alpha_i}{d_i}}. \tag{17}$$

The sum runs over all MUSIG groups i which belong to the velocity group j. Based on this Sauter mean diameter the heat transfer coefficients and interfacial area density are calculated resulting in a value for the mass transfer per unit volume and time for velocity group j Γ_j. The mass transfer for the MUSIG groups i is obtained by:

$$\Gamma_i = \Gamma_j \frac{a_i}{a_j} = \Gamma_j \frac{\frac{6\alpha_i}{d_i}}{\frac{6\alpha_j}{D_{S,j}}} = \Gamma_j \frac{\alpha_i}{\alpha_j}\frac{D_{s,j}}{d_i}. \tag{18}$$

These extensions of the Inhomogeneous MUSIG model were recently implemented into the CFD code CFX from ANSYS. Presently first tests are done to verify the implementation.

3. THE NEW EXPERIMENTAL SETUP

Experiments are done using the TOPFLOW facility of the Forschungszentrum Dresden-Rossendorf. The facility allows to produce up to 1.4 kg steam per second at the maximum operational pressure of 7 MPa by a 4 MW electrical steam generator [13]. Several test rigs are operated at the facility. For investigations of two-phase flow characteristics in vertical pipes

wire-mesh sensors are used. This technology, shortly described in section 3.2, is intrusive, i.e. it influences the two-phase flow. For this reason it is not possible to place several sensors behind each other to investigate the evolution of the flow along the pipe. Instead in the experiments to investigate the evolution of the flow the measuring plane is always at the upper end of the pipe and gas is injected at different distances from this measuring plane through orifices in the pipe wall. This so-called Variable Gas Injection setup is presented in the following section.

3.1 Variable Gas Injection

For the condensation experiments the so-called Variable Gas Injection device [6] is used. Compared to previous experiments described by Lucas and Prasser [11] some extensions were implemented. The scheme of the new setup is shown at Fig. 1a. The test section consists of a vertical steel pipe with an inner diameter of 195.3 mm and a length of about 8 m. The measurement plane which consists of a pair of wire-mesh sensors and a lance with thermo-couples is located at the upper end of the test section. The device is equipped with seven gas injection units which allow to inject air or steam via orifices in the pipe wall. The gas injection via wall orifices offers the advantage that the two-phase flow can rise smoothly to the measurement plane, without being influenced by the feeder within the tube in other height positions. The injection devices are arranged almost logarithmically over the pipe length since the flow structure varies quite fast close to the gas injection mainly caused by the radial redistribution of the gas. Six of the gas injection modules (Fig. 1c) consist of three injection chambers. Two of the three chambers (the uppermost and the lowest) have 72 x 1 mm orifices. The middle chamber has 32 x 4 mm orifices, which is used to vary the initial bubble size distribution. For rotation–symmetric gas injection, all orifices per chambers are equally distributed over the circumference of the pipe. The injection chambers themselves were designed to guarantee an equal gas feeding by all the orifices and are operated separately. For the condensation experiments an additional injection chamber with 1 mm orifices is installed as close to the measuring plane as possible (36 mm between gas injection plane and measurement plane of the first wire-mesh sensor in flow direction; L/D ~ 0.2). This was done to provide more detailed information on the injected steam bubbles. Only one injection chamber is activated for a single measurement.

The supply of the liquid phase is done from the bottom of the test section by means of an isolating valve and a 90° bend. The test section pump circulates the saturated water from the steam drum to the lower end of the variable gas injection. In addition cold water is injected through a mixing device at the lower end of the test section. This allows to obtain a sub-cooling of the water of several Kelvin depending on the flow rates. This sub-cooling is adjusted by thermocouples, mounted in the saturated water pipe as well as in the Variable Gas Injection pipe below the injection levels R and O for the mixing temperature (see Fig. 1a).

In contrast to the previous experiments [11] the nominal pressure is now set at the position of the respectively activated injection chamber. Thus switching between different positions of the injection provides the same conditions like in case of a fixed location of the injection and shifting the measuring plane. This especially important for the condensation experiments since saturation temperature and with that also sub-cooling depends on pressure. To adjust the pressure the absolute value is measured at the upper end of the test section. In addition the differential pressure between this measurement position and the position of the single gas injection is determined (see Fig. 1a).

In addition to the measurement of the two-phase flow characteristics by wire-mesh sensors as described in the following section, also information on local temperatures is required. For this reason a lance of thermocouples is mounted directly above the wire-mesh sensor. It spans over the whole pipe diameter. The single positions of the thermocouples can be assigned to single measuring points of the wire-mesh sensor. This allows to combine the information on local void fraction and local temperature and allows to determine the liquid temperature from measured mixture temperature by correlating the temporal signals of both measurements.

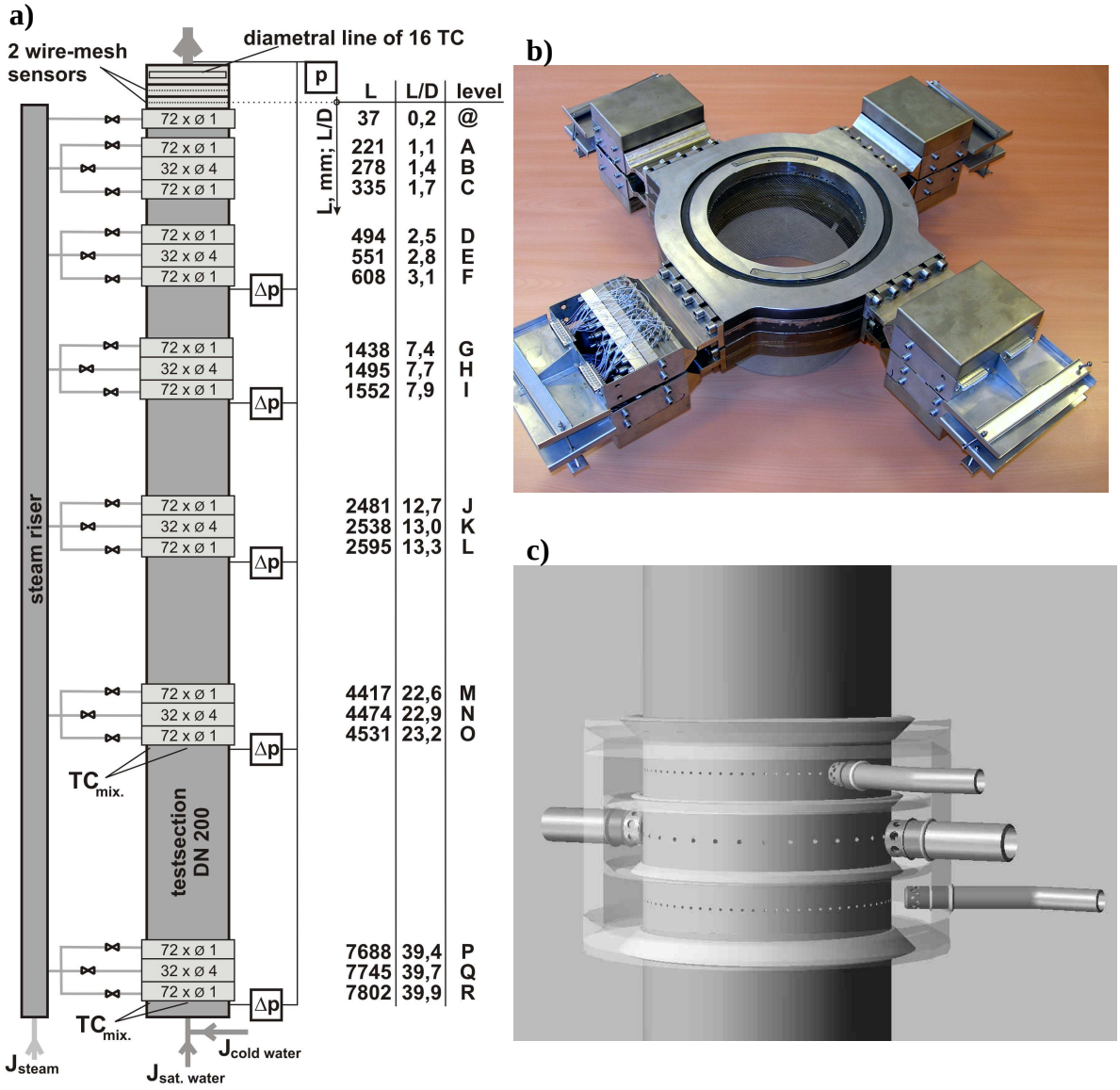

Fig. 1 Variable Gas Injection: a) Scheme of the test section, b) wire-mesh sensors, c) gas injection module

3.2 Wire-mesh sensors

Numerous papers were published in the past on the wire-mesh sensor technology (e.g. [13, 14]) and on experiments using the wire-mesh sensor (e.g. [3, 6, 11, 16]). For this reason here only the basic principle is presented. A wire-mesh sensor consists of two grids of parallel

wires, which span over the measurement cross-section. The wires of both planes cross under an angle of 90°, but do not touch. Instead there is a vertical distance between the wires at the crossing points. At these points the conductivity is measured. According to the different conductivity of gas and water the phase present in the moment of the measurement at the crossing point can be determined. Many different types of wire-mesh sensors were built and successfully used during the last 15 years. Some error estimation is given in [10].

In the present case, two new developed high temperature wire-mesh sensors were employed (Fig. 1b). They are designed for an operational pressure up to 7 MPa and the corresponding saturation temperature of 286°C. Each plane of the sensor is composed of 64 x 64 wires that have a lateral pitch of 3 mm. The distance between the two grid levels is app. 3 mm. Due to thermal expansion it is necessary to stress each single wire by a spring. A disadvantage of the previous wire-mesh sensor design was the occurrence of leakages at high pressures. For this reason the present sensor seals each of the 128 wire electrodes with a single packing box. Inside these boxes employed a new synthetic material which allows the electrical and pressure insulation simultaneous up to high temperatures. Additionally, the packing boxes simplify the replacement of damaged wires. Furthermore the body of the sensor is designed modular. This feature reduces the weight of the sensor essential and simplifies the maintenance. One further improvement was the reduction of the diameter of the wire electrodes to 100 µm, whereby the obstruction of the flow cross section decreases below the half compared to the previous construction.

Measurements were done with a frequency of 2500 frames per second, i.e. 2500 pictures of the instantaneous gas distribution in the pipe cross section are obtained. The measuring time was 10 s for each single measurement, i.e. the result of one measurement is a three-dimensional matrix of 64*64*25.000 values of the instantaneous local conductivity. By a calibration procedure a matrix of the instantaneous local volume void fraction with the same dimensions is calculated.

The 64*64*25.000 matrix of void fraction values can be visualized to provide an impression of flow characteristics. More important is the generation of quantitative data by using averaging procedures. Most important is the time averaging, which e.g. leads to time averaged two-dimensional gas volume fraction distributions in the pipe cross section. Due to the radial symmetry of the data the statistical error can be further lowered by an azimuthally averaging. To do this the cross section is sub-divided into 80 ring-shaped domains with equal radial width. The contribution of each mesh is calculated by weight coefficients obtained from a geometrical assignment of the fractions of a mesh belonging to these rings. In the result **radial gas volume fraction profiles** are obtained.

For the measurements two sensors were used which measurement planes have a distance of 40 mm. This allows to cross-correlate the gas volume fraction values of the two-planes for all mesh point which are located above each other. From the maxima of the cross-correlation functions the typical time shift of the local void fraction fluctuations can be determined. Since the distance between the measuring planes is known the local time averaged gas velocity can be calculated. The point-to-point two-dimensional gas velocity distributions in the pipe cross section are obtained in the results of this procedure. Again an azimuthally averaging is applied to obtain the **radial profiles of the gas velocity**. Please consider, that the second sensor is only used for the determination of the gas velocities. Due to the perturbing effect of the first sensor other data as especially bubble size distributions obtained from the second sensor would be distorted.

The next step of the data evaluation procedure is the identification of single bubbles. Thereby, a bubble is defined as a region of connected gas-containing elements in void fraction matrix which is completely surrounded by elements containing the liquid phase. A complex procedure, described in [15], applies a filling algorithm combined with sophisticated stop criteria to avoid artificial combinations as well as artificial fragmentation of bubbles. In the result to each element which belongs to one bubble, the same identification number is assigned. Different bubbles receive different identification numbers. These numbers are stored in the elements of a second array. This array has the same dimension as the void fraction array. Combining the information from the void faction and bubble number arrays together with the radial profiles of the gas velocity characteristic data of the single bubbles as bubble volume, sphere equivalent bubble diameter, maximum circle equivalent bubble diameter in the horizontal plane, coordinates of the bubble centre of mass, moments characterizing asymmetries and others are obtained. Based on these data cross section and time averaged **bubble size distributions** and **radial gas volume fraction profiles decomposed according to the bubble size** are calculated. The bubble size distributions are defined volume fraction related, i.e. they present the volume fraction per width of a bubble diameter class (equivalent diameter of a sphere with the measured bubble volume V_b is considered).

4. FIRST PRELIMINARY EXPERIMENTAL RESULTS

A first experimental run was done aiming on test and optimization of the experimental procedure. This concerns the controllability of the flow rates, pressure, temperatures and other parameter. The achievable accuracy of the set values was tested as well as the correct interplay of the measuring technique.

To set the aspired pressure at the location of the respectively activated steam injection chamber – which was 1 MPa for this first run - the pressure in the steam drum has to be changed. Since the saturated water is taken from the steam drum, the temperature of the feedwater injected at the lower end of the test section changes for different steam injection positions. In this first test the flow rate of both, the saturated and cold water streams were kept constant resulting in a total water flow rate of 0.032 m^3/s which correspond to a superficial velocity of 1.067 m/s. In the result the sub-cooling varied for the different injection position and was in the range of 2 – 4K. To guarantee the same sub-cooling for all measured L/D the change of the temperature of the feedwater has to be compensated by the flow rate of the injected cold water. At the same time the total water flow rate has also to be kept constant. The achievable accuracy of these settings were also tested.

Steam was injected with a mass flow rate of 80 g/s. The corresponding superficial velocity is 0.53 m/s. Fig. 2 shows the decrease of the gas volume fraction along the pipe due to bubble condensation. The curves show the expected trends and fit to the results obtained in previous experiments [11]. Due to the large bubbles, i.e. smaller interfacial area density the condensation is slower in case of the steam injection through 4 mm orifices. Fig. 3 shows a comparison for the evolution of the radial gas volume fraction with increasing L/D. As shown in Fig. 1 only for the 1 mm injection a chamber very close to the wire mesh sensor is available. Obviously the steam is blown into the pipe as a gas jet leading to a maximum of this profile away from the wall (black curve in Fig. 3). Due to secondary flows the bubbles seem to migrate first towards pipe wall, before they start to distribute over the pipe cross-section. Further investigations are necessary to clarify these effects.

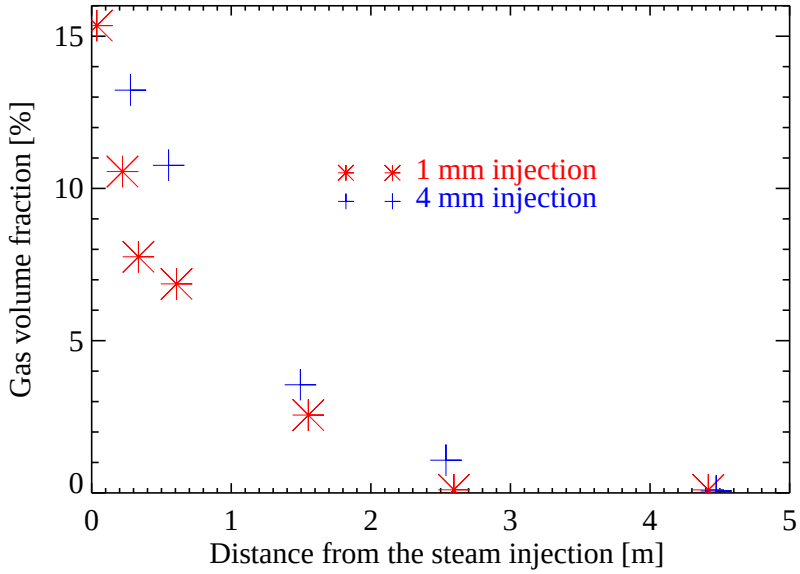

Fig. 2 Evolution of the time and cross-section averaged gas volume fraction along the pipe for two different steam injection orifice sizes.

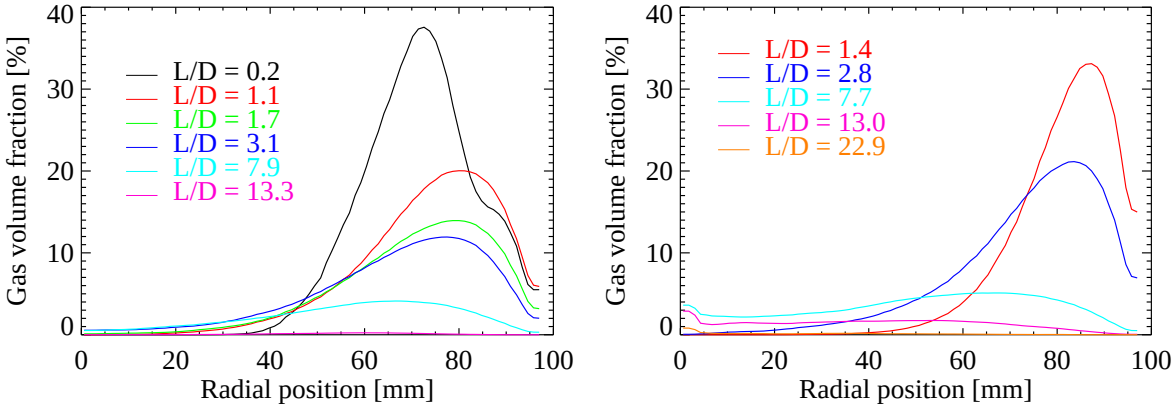

Fig. 3 Evolution of the radial gas volume fraction profiles along the pipe for steam injection through 1 mm orifices (left) and 4 mm orifices (right).

5. CONCLUSIONS

A proper simulation of poly-dispersed flows has to consider local and time-dependent bubble size distributions. The Inhomogeneous MUSIG model which has been recently implemented into the CFD code CFX allows the definition of bubble size classes regarding the mass balance but also regarding the momentum balance. Up to now transfers between the groups are considered only due to bubble coalescence and breakup. In case of flows with phase transfer additional source terms have to appear in the balance equations for these bubble size groups. The derivation of the corresponding extensions of the MUSIG model are presented in the paper. They are presently implemented into the CFX code. For a first validation experimental data on condensing poly-dispersed bubbly flow in a large vertical pipe will be used. The experimental setup and preliminary results are also presented. Due to the detailed information on the local structure of the interface obtained by wire-mesh sensor measurements the data are suitable for such a validation.

ACKNOWLEDGMENTS

This work is carried out in the frame of a current research project funded by the German Federal Ministry of Economics and Labor, project numbers 150 1328 and 150 1329. The authors like to thank all members of the TOPFLOW team who contributed to the successful performance of these experiments.

REFERENCES

1. T. Höhne, S. Kliem, U. Rohde, F.-P. Weiss, “Buoyancy driven coolant mixing studies of natural circulation flows at the ROCOM test facility using ANSYS CFX”, *Nuclear Engineering and Design*, **238**, pp. 1987-1995 (2008).
2. D. Lucas, D. Bestion, et al., “An overview of the Pressurized Thermal Shock issue in the context of the NURESIM project”, *Science and Technology of Nuclear Installations*, **2009**, 583259 (2008)
3. D. Lucas, E. Krepper, H.-M. Prasser, “Use of models for lift, wall and turbulent dispersion forces acting on bubbles for poly-disperse flows”, *Chemical Science and Engineering*, **62**, pp. 4146-4157 (2007).
4. A. Tomiyama, “Struggle with computational bubble dynamics”, *3rd Int. Conf. on Multiphase Flow, ICMF'98*, Lyon, France (1998).
5. D. Lucas, E. Krepper, H.-M. Prasser, “Prediction of radial gas profiles in vertical pipe flow on basis of the bubble size distribution”, *International Journal of Thermal Sciences*, **40**, pp. 217-225 (2001).
6. H.-M. Prasser, et al., “Evolution of the structure of a gas–liquid two-phase flow in a large vertical pipe”, *Nuclear Engineering and Design*, **237**, pp. 1848–1861 (2007).
7. E. Krepper, D. Lucas, H.-M. Prasser, “On the modelling of bubbly flow in vertical pipes”, *Nuclear Engineering and Design*, **235**, pp. 597-611 (2005).
8. T. Frank, et al., “Validation of CFD models for mono- and polydisperse air-water two-phase flows in pipes”, *Nuclear Engineering and Design*, **238**, pp. 647-659 (2008).
9. E. Krepper, et al., “The inhomogeneous MUSIG model for the simulation of polydispersed flows”, *Nuclear Engineering and Design*, **238**, pp. 1690-1702 (2008).
10. D. Lucas, et al., “Benchmark database on the evolution of two-phase flows in a vertical pipe”, *XCFD4NRS, Experiments and CFD Code Applications to Nuclear Reactor Safety*, 10.-12.09.2008, Grenoble, France, (2008).
11. D. Lucas, H.-M. Prasser, “Steam bubble condensation in sub-cooled water in case of co-current vertical pipe flow”, *Nuclear Engineering and Design*, **237**, pp. 497-508 (2007).
12. P.M. Carrica, et al., “A polydisperse model for bubbly two-phase flow around a surface ship”, *International Journal of Multiphase Flow*, **25**, pp. 257-305 (1999).
13. H.-M. Prasser, et al., “The multipurpose thermal-hydraulic test facility TOPFLOW: an overview on experimental capabilities, instrumentation and results”, *Kerntechnik*, **71**, pp. 163-173 (2006).
14. H.-M. Prasser, et al., “A new electrode-mesh tomograph for gas/liquid flows”, *Flow Measurement and Instrumentation*, **9**, pp. 111 – 119 (1998).
15. H.-M. Prasser, et al., “Bubble size measurement using wire-mesh sensors”, *Flow Measurement and Instrumentation*, **12**, pp. 299-312 (2001).
16. D. Lucas, et al., “Development of co-current air–water flow in a vertical pipe”, *International Journal of Multiphase Flow*, **31**, pp. 1304–1328 (2005).